Computer Methods in Applied Mechanics and Engineering 433 (2025) 117525

Contents lists available at ScienceDirect

Comput. Methods Appl. Mech. Engrg.

journal homepage: www.elsevier.com/locate/cma

Direct data-driven algorithms for multiscale mechanics

E. Prume [a,*], C. Gierden [b], M. Ortiz [c,d], S. Reese [a,e]

[a] Institute of Applied Mechanics, RWTH Aachen University, Mies-van-der-Rohe-Str. 1, D-52074 Aachen, Germany
[b] Institute of Mechanics of Materials, Ruhr University Bochum, Universitätsstrasse 150, D-44801 Bochum, Germany
[c] Hausdorff Center for Mathematics, Universität Bonn, Endenicher Allee 60, 53115 Bonn, Germany
[d] Division of Engineering and Applied Science, California Institute of Technology, 1200 E. California Blvd., Pasadena, CA 91125, USA
[e] University of Siegen, Adolf-Reichwein-Str. 2a, D-57076 Siegen, Germany

ARTICLE INFO

Keywords:
Data-Driven
Computational mechanics
Multiscale mechanics
Algorithms

ABSTRACT

We propose a randomized data-driven solver for multiscale mechanics problems which improves accuracy by escaping local minima and reducing dependency on metric parameters, while requiring minimal changes relative to non-randomized solvers. We additionally develop an adaptive data-generation scheme to enrich data sets in an effective manner. This enrichment is achieved by utilizing material tangent information and an error-weighted k-means clustering algorithm. The proposed algorithms are assessed by means of three-dimensional test cases with data from a representative volume element model.

1. Introduction

In this work, we consider two-scale problems where the finer scale is characterized by a representative volume element (RVE) that captures the details of the material microstructure and serves as a local material description of a macroscopic, mechanical boundary value problem (BVP). This type of material modeling is referred to as *upscaling* [1,2]. In the FE^2 method [3], the RVE is evaluated at every material point, time step and possibly multiple iterations, which can be exceedingly costly. To reduce the number of RVE evaluations in an inelastic setting, [4] developed a k-means clustering FE^2 approach where material points of similar deformation behavior are grouped and jointly evaluated.

Another popular approach is to perform a series of evaluations (or "virtual experiments") with an RVE model and calibrate a phenomenological material model to the resulting data set. More recently, the material modeling is often performed by specialized *supervised* neural network architectures in order to automatize and standardize the modeling procedure for elastic [5,6] and inelastic [7,8] material behavior, see for instance [9,10] for a review. A number of methods have been developed in order to reduce the number of RVE evaluations and improve the accuracy of the trained material model [11,12].

The advantage of the supervised approach is the fast model evaluation, while the disadvantage is that additional modeling uncertainties are introduced by biased modeling assumptions, including which and how many virtual experiments are performed, how validation and verification are performed and what features and functional basis are chosen for the model. Thus, when performing a predictive computation, i. e., a previously unseen material state, with a calibrated model, it is often not clear whether the local response of the material model needs to be validated by an RVE evaluation or may be assumed to be reliable. In addition, the cost of training the neural network architectures, while often not accounted for, can be very high, especially with large data sets and high-dimensional data.

In order to eschew these shortcomings of supervised models, in direct, or *unsupervised*, data-driven methods a pre-existing material data set is directly used in the solution of the boundary-value problem [13]. In this manner, only actual unbiased RVE data are used

* Corresponding author.
E-mail address: erik.prume@ifam.rwth-aachen.de (E. Prume).

https://doi.org/10.1016/j.cma.2024.117525
Received 30 June 2024; Received in revised form 31 October 2024; Accepted 31 October 2024
Available online 12 November 2024

for purposes of material characterization. Evidently, the accuracy of the solution depends on the degree of coverage supplied by the material data set, which can be efficiently monitored using a distance function [13–15]. This quantitative metric can be used to identify regions of insufficient data coverage and to develop strategies to acquire new data in a systematic manner.

The direct data-driven method has been extended to large deformations [16,17], inelastic material behavior [18,19] and uncertainty quantification [20–22]. To improve the accuracy with sparse data sets, [23,24] include material tangent information in the solving process. Furthermore, the method has been applied to other field equations than mechanics, such as magnetism [25] or electro-mechanical coupled problems [26]. In [27], the direct data-driven method has been reformulated in order to identify stress data from a sequence of strain field measurements. Similarly, [28] proposes an automated discovery scheme for plastic material laws using only strain data.

While this paper aims to enable efficient multiscale computations with synthetic microstructures, the direct data-driven method has been also used with real data measurements, based on the identification of two-dimensional stress fields [29–31] using Digital Image Correlation (DIC) measurements. Particularly challenging, but not impossible, is obtaining strain data in the three-dimensional case using Digital Volume Correlation (DVC) measurements [32], which in turn can be used to identify the corresponding stress data. Furthermore, domain specific measurement techniques are used to obtain real 3D data, see for example [33] which uses elastography data for a viscoelastic biomechanical problem.

This paper has two novel, significant improvements over previous work. First, it tackles the long-standing problem of finding the global optimizer of the double minimization problem [13] which was also reported in [34–36]. This problem is in particular relevant for rather sparse data sets with three-dimensional, nonlinear material behavior. We propose a simple variation of the original fixed-point algorithm that effectively helps to escape local minima and reduces the dependence on the choice of metric coefficients. Compared to previous works, the particular advantages of the proposed approach are that it is easy to implement and does not increase the computational effort, yet is effective. Second, we contribute an incremental improvement for the systematic data acquisition problem in the multiscale context compared to previous work [15,37]. In particular, we show how to exploit the material tangent information and the intrinsic error measure of the direct data-driven approach using a weighted k-means algorithm. The result is an effective and consistent data set enrichment scheme for nonlinear and path-dependent, force and displacement driven problems, thus minimizing the number of costly RVE evaluations in an unsupervised manner.

The paper is structured accordingly: in Section 2, we briefly review the theory of direct data-driven mechanics; in Section 3 the improved solver is formulated and tested on a numerical example; in Section 4 the adaptive data generation scheme is developed and evaluated with the aid of a numerical example. Finally, in Section 5 we summarize our findings and provide an outlook for further work.

2. Preliminaries: Direct data-driven mechanics

In this section, we provide a compact review of the direct data-driven computing paradigm as proposed by [13] and the notation used in the following sections. We consider discretized mechanical systems of m material points, each characterized by a strain state $\varepsilon_e \in \mathbb{R}^d$, a stress state $\sigma_e \in \mathbb{R}^d$ and a volume $w_e \in \mathbb{R}$. Hereby, the index e indicates the specific material point and d is the dimension of stress and strain, that is $d = 6$ in the considered three-dimensional, geometrical linear case. In addition, we define the weighted Euclidean norms $\|\varepsilon_e\|^2 := \varepsilon_e \cdot \mathbb{C}_e \varepsilon_e$ and $\|\sigma_e\|^2 := \sigma_e \cdot \mathbb{C}_e^{-1} \sigma_e$ in order to account for different units of stresses and strains. The matrix $\mathbb{C}_e$ contains metric coefficients whose influence is studied in Section 3.

The idea of the direct data-driven approach is to formulate the solution of the boundary value problem explicitly in the given experimental stress–strain data, which is given in the form of local data set(s)

$$D_e = \{(\varepsilon'_i, \sigma'_i)\}_{i=1}^{n_e} \tag{1}$$

with n_e material data points. The direct data-driven solution is then defined as that assignment of data points to each material point which fulfills the physical constraints of force equilibrium and kinematical compatibility simultaneously in an optimal sense.

We describe the kinematical compatibility by the set

$$E_\varepsilon := \left\{(\varepsilon_1, \dots, \varepsilon_m) \in \mathbb{R}^{md} \,:\, \varepsilon_e = B_e u,\ e = 1, \dots, m\right\} \tag{2}$$

of all strain fields $\varepsilon \in E_\varepsilon$ which are derived from displacement fields $u \in \mathbb{R}^n$ by the geometrical discretized gradient operator $B_e \in \mathbb{R}^{d \times n}$. Hereby, n is the number of degrees of freedom of the overall system including boundary conditions. Similarly, the force equilibrium is described by the set

$$E_\sigma := \left\{ (\sigma_1, \dots, \sigma_m) \in \mathbb{R}^{md} \,:\, \sum_{e=1}^{m} w_e B_e^T \sigma_e = f \right\} \tag{3}$$

of all stress fields $\sigma \in E_\sigma$ which fulfill the discretized force equilibrium given a force field $f \in \mathbb{R}^n$. Similarly to the local norms, we define $\|\varepsilon\|^2 := \sum_{e=1}^m w_e \|\varepsilon_e\|^2$ and $\|\sigma\|^2 := \sum_{e=1}^m w_e \|\sigma_e\|^2$ as the global norms accounting for the different material point volumes w_e.

Formally, we denote the set of all possible assignments of data points to material points by

$$D = D_1 \times D_2 \times \dots \times D_m \tag{4}$$

and one such assignment by $(\varepsilon', \sigma') = ((\varepsilon'_{e=1}, \dots, \varepsilon'_{e=m}), (\sigma'_{e=1}, \dots, \sigma'_{e=m})) \in D$. We note that Eq. (2) and (3) constrain the strain and stress fields independently of each other and the coupling between the two fields is only established by the material data set.

Using these notations, the direct data-driven problem can be formulated by

$$\min_{(\varepsilon',\sigma')\in D}\left(\min_{\varepsilon\in E_\varepsilon}\|\varepsilon-\varepsilon'\|^2+\min_{\sigma\in E_\sigma}\|\sigma-\sigma'\|^2\right) \tag{5}$$

with an optimal data assignment (ε',σ') and its corresponding, closest admissible strain and stress fields (ε,σ) as the solution.

For the computation of the closest compatible strain field and the closest equilibrium stress field we introduce the two projection operations $P_\varepsilon(\varepsilon')=\arg\min_{\varepsilon\in E_\varepsilon}\|\varepsilon-\varepsilon'\|^2$ and $P_\sigma(\sigma')=\arg\min_{\sigma\in E_\sigma}\|\sigma-\sigma'\|^2$ which consists in solving two linear, decoupled systems of equations

$$\left[B_{\text{red}}^T W\mathbb{C}B_{\text{red}}\right]u_{\text{red}}=B_{\text{red}}^T\mathbb{C}\varepsilon' \tag{6a}$$

$$\left[B_{\text{red}}^T W\mathbb{C}B_{\text{red}}\right]\eta_{\text{red}}=f_{\text{red}}-B_{\text{red}}^T W\sigma'. \tag{6b}$$

Here B_{red} is the assembled, discretized gradient operator, or B-operator after removing the degrees of freedom associated to Dirichlet boundary conditions, $W=\text{diag}(w_0,w_1,\dots,w_m)$ the material point volumes, $\mathbb{C}=\text{diag}(\mathbb{C}_1,\mathbb{C}_2,\dots,\mathbb{C}_m)$ the metric coefficients and f the applied external force vector.

From the two solutions of Eq. (6) the projection operations follow as

$$P_\varepsilon(\varepsilon')=Bu \tag{7}$$

$$P_\sigma(\sigma')=\sigma'+\mathbb{C}B\eta. \tag{8}$$

Note that B denotes the assembled B-operator including the degrees of freedom accounting for boundary conditions. Also, u contains u_{red} as well as the applied Dirichlet boundary conditions and η contains η_{red} as well as zeros at the constraint degrees of freedom.

For the two projection operations involved, *i.e.* the computation of the closest compatible strain field $P_\varepsilon(\varepsilon')=\arg\min_{\varepsilon\in E_\varepsilon}\|\varepsilon-\varepsilon'\|^2$ and the closest equilibrium stress field $P_\sigma(\sigma')=\arg\min_{\sigma\in E_\sigma}\|\sigma-\sigma'\|^2$ only two linear, decoupled system of equations have to be solve.

It is important to realize that the number of possible data assignments $|D|=\Pi_{e=1}^m n_e$ is of combinatorial complexity and a solution to problem (5) is not directly computable. Therefore, several heuristic solver schemes has been proposed. The fixed-point solver proposed by [13] which we call in the following the "original fixed-point solver" is summarized in Alg. 1.

Algorithm 1 Original Fixed-Point Solver

Require: Constraint set $E=E_\varepsilon\times E_\sigma$.
Require: Local data set(s) $D_e=\{(\varepsilon_i',\sigma_i')\}_{i=1}^{n_e}$.
Require: Convergence tolerance TOL
  Initialize: $(\varepsilon',\sigma')\in D$ randomly
  Initialize: $F_0\leftarrow 0, F\leftarrow\infty$
  while $|F-F_0|<\text{TOL}$ **do**
    Set: $\varepsilon\leftarrow P_\varepsilon(\varepsilon')$
    Set: $\sigma\leftarrow P_\sigma(\sigma')$
    Set: $F_0\leftarrow F$
    Set: $F\leftarrow\frac{1}{m}\sum_{e=1}^m\left(\|\varepsilon_e-\varepsilon_e'\|+\|\sigma_e-\sigma_e'\|\right)$
    for $e=1\dots m$ **do**
      Set: $(\varepsilon_e',\sigma_e')\leftarrow\arg\min_{(\varepsilon_i',\sigma_i')\in D_e}\left(\|\varepsilon_e-\varepsilon_i'\|^2+\|\sigma_e-\sigma_i'\|^2\right)$
    end for
  end while
  return $(\varepsilon',\sigma'),(\varepsilon,\sigma)$

3. Randomized fixed-point solver: An alternative solver scheme

3.1. Motivation

The first contribution is an enhancement of the original solver scheme summarized in Alg. 1, which is beneficial for all kind of data-driven problems within the present framework. As also reported in [34,36], the original solver fails to find the global minimizer of the optimization problem, in particular in the case of sparse data sets. In addition, the accuracy depends on the metric parameter $\mathbb{C}_e$, which has to be chosen in advance. To improve the accuracy, [34] proposes a mixed-integer global optimization technique, which becomes however computationally inefficient for larger systems. More closely to the original algorithm, [36,38] proposes to adapt the metric coefficient online in an adaptive way in order to improve convergence properties, which requires however to assemble the stiffness matrix and build the data search structures multiple times during the online computation and additional local fitting procedures.

3.2. Proposed method: Randomized fixed-point solver

We propose a variation of the original algorithm that overcomes the aforementioned issues while requiring only minimal changes. The basic idea of the algorithm is to perform the data search separated for stresses and strains in each material point in a randomized manner. In contrast to the original algorithm, which assigns to each material point the data point that minimizes simultaneously the distance of stresses and strains, our proposed algorithm searches only for the data which is closest with respect to *either* stresses *or* strains. If a given material point executes a strain search (and not a stress search), it is decided randomly with probability $p = 1/2$ at each iteration. Since we cannot expect that the error will decrease in every iteration, it is necessary to adapt the convergence criteria. The algorithm will be terminated if the optimal solution cannot be further improved after a certain number of iterations. The algorithm is summarized in Alg. 2.

Algorithm 2 Randomized Fixed-Point Solver

Require: Constraint set $E = E_\varepsilon \times E_\sigma$.
Require: Local data set(s) $D_e = \{(\varepsilon'_i, \sigma'_i)\}_{i=1}^{n_e}$.
Require: Maximum number of iterations with increasing error n_{trial}
  Initialize: $(\varepsilon', \sigma') \in D$ randomly
  Initialize: $F_{\min} \leftarrow \infty$
  $j_{\min} = 0, j = 0$
  while $j < j_{\min} + n_{\text{trial}}$ **do**
    Set: $\varepsilon \leftarrow P_\varepsilon(\varepsilon')$
    Set: $\sigma \leftarrow P_\sigma(\sigma')$
    Set: $F \leftarrow \frac{1}{m}\sum_{e=1}^{m} \left(\|\varepsilon_e - \varepsilon'_e\| + \|\sigma_e - \sigma'_e\|\right)$
    if $F < F_{\min}$ **then**
      Set: $F_{\min} \leftarrow F$
      Set: $j_{\min} \leftarrow j$
    end if
    Set: $j \leftarrow j + 1$
    for $e = 1 \dots m$ **do**
      Set: $r \sim \text{Ber}(1/2)$ #Bernoulli random variable
      if r = 0 **then**
        Set: $(\varepsilon'_e, \sigma'_e) \leftarrow \arg\min_{(\varepsilon'_i, \sigma'_i) \in D_e} \|\varepsilon_e - \varepsilon'_i\|^2$
      else
        Set: $(\varepsilon'_e, \sigma'_e) \leftarrow \arg\min_{(\varepsilon'_i, \sigma'_i) \in D_e} \|\sigma_e - \sigma'_i\|^2$
      end if
    end for
  end while
  return $(\varepsilon', \sigma'), (\varepsilon, \sigma)$

3.3. Numerical example: Stamp

3.3.1. Setup

We compare the proposed randomized fixed-point solver with the original fixed-point solver by means of a numerical example. The considered boundary value problem is shown in Fig. 1. The data set in this section is set to the reference solution using a three-dimensional von-Mises plasticity material model with linear isotropic hardening containing 34,606 data points.

The material parameters are chosen as follows: Young's modulus $E = 1000.0$[MPa], Poisson's ratio $\nu = 0.3$, hardening modulus $H = 100.0$[MPa] and initial yield strength $\sigma_{y0} = 25.0$[MPa]. The shear loading $\bar{u}(t) = (10t/t_{\max}, 0, 0)$ is applied in 10 load steps. The finite element mesh consists of 3146 linear tetrahedral elements in three dimensional space.

3.3.2. Results

First, we investigate the influence of the metric coefficients $\mathbb{C}_e = cI$, where we set the metric tensor proportional to the identity matrix. We consider a single time step at $t = 0.5t_{max}$. The error is defined by the mean distance of the converged solution (ε', σ') to the reference solution $(\varepsilon_{\text{ref}}, \sigma_{\text{ref}})$ as $\mathcal{E}_{\text{ref}} = \frac{1}{m}\sum_{e=1}^{m} \left(\|\varepsilon_{e,\text{ref}} - \varepsilon'_e\| + \|\sigma_{e,\text{ref}} - \sigma'_e\|\right)$ using a fixed reference metric $\mathbb{C}_{e,\text{ref}} = 1000I$ so that the error measurement is independent of the metric parameter and thus comparable for different choices of c. Since the reference solution is included in the data set, we ideally expect any data-driven solver scheme to find a solution which satisfies equilibrium and compatibility up to numerical precision of the data. The results shown in Fig. 2 (A) depicts the dependency of the original solver scheme on the metric coefficient c. Additionally, the original algorithm fails to find the global minimizer even for an optimal choice of the metric. In contrast, remarkably, the proposed randomized solver scheme computes independently of the chosen metric an almost optimal solution. Performing 30 independent runs, the original algorithm achieves in the best case for $c = 1000$ an error of 0.55 while the randomized solve achieves on average over all choices of c an error of $2.2 \cdot 10^{-5}$ with a standard deviation of $2.0 \cdot 10^{-4}$. These measures are heavily influenced by the outliers which does not find the exact solution: 423 out of 450 (15 different metrics times 30 samples each) computations have an error below 10^{-16} meaning that the exact reference solution was found in these

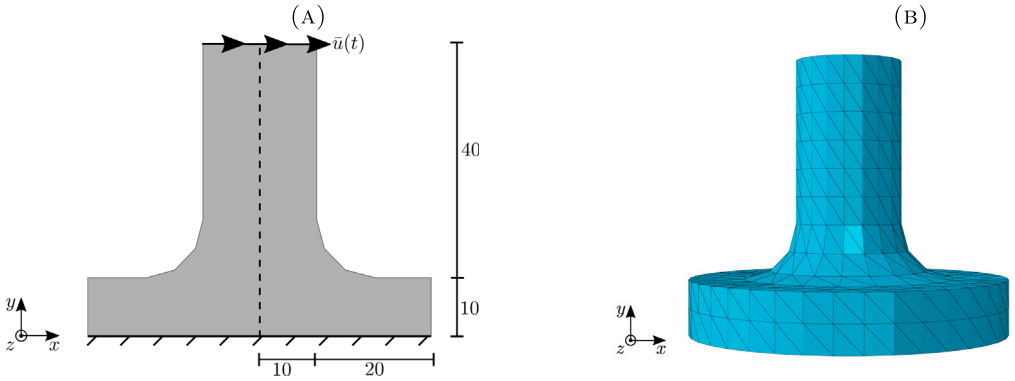

Fig. 1. Stamp boundary value problem.

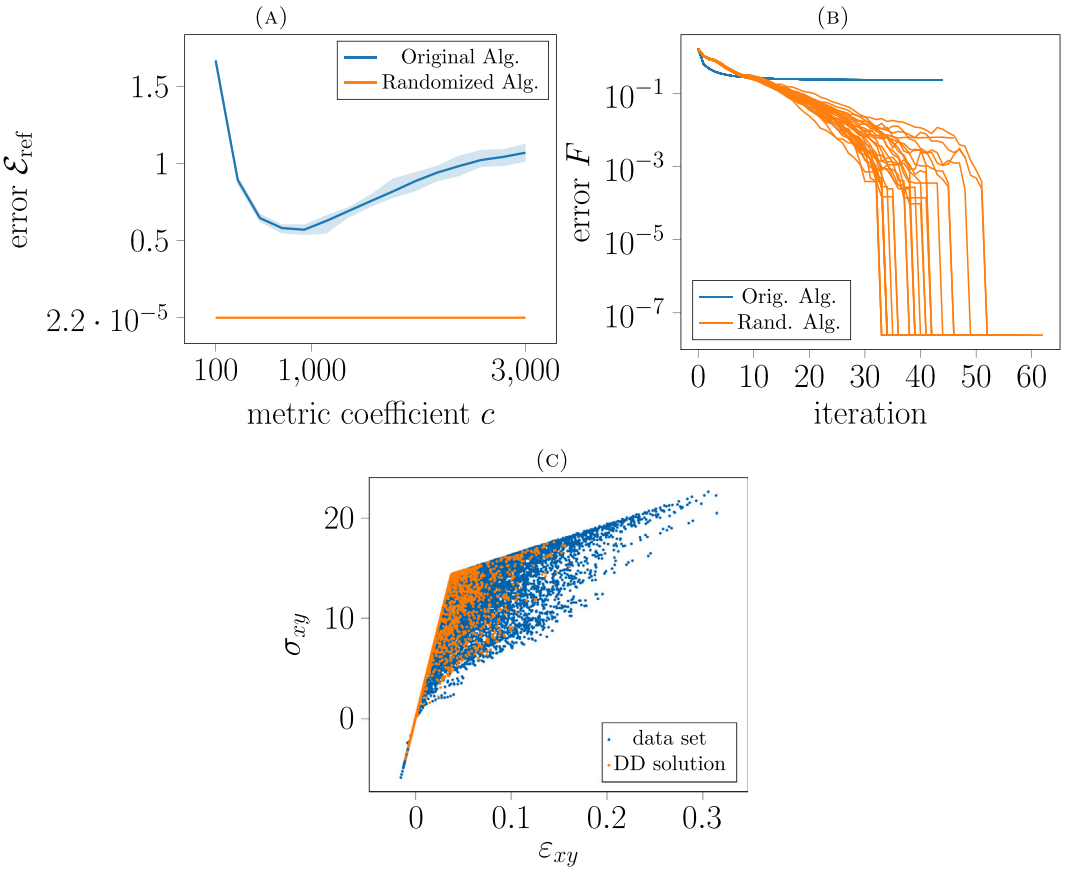

Fig. 2. (A) Influence of the metric parameter on the original and randomized algorithm. Shaded areas denote the maximum deviations from the mean of 30 independent runs. (B) Error in constraints during the iterations for both algorithms for $c = 1000$. (C) Blue: Local data set, orange: optimal data point assignment of each material point.

cases. Thus, the randomized solver finds independently of the metric coefficient c in most runs the optimal solution. In Fig. 2 (B) the evolution of the error during the iterations is shown for both algorithms for $c = 1000$. While the original algorithm takes in the first iterations large steps towards the minimum, it cannot effectively escape local minima. The randomized algorithm starts slower and does not necessarily decrease the error in each iteration, however, it has the capability to compute almost optimal solutions. Fig. 2 (C) visualizes the local data set and the computed solution of optimal data assignments of each material point.

The randomized solver comes with no computational overhead. The computation time per iteration for the original algorithm is on average 0.034 [s] and 0.025 [s] for the randomized algorithm. One explanation for this is that the data search in the

randomized algorithm is distributed to two search structures of dimensionality 6 (dimension of stress/strain) instead of a single search structures of dimensionality 12, without adding any additional number of search operations. In addition, we emphasize that only minimal changes are required to implement the proposed randomized fixed-point solver with respect to the original fixed-point solver [13]. Nevertheless, we observe significant improvements in both accuracy and robustness with respect to the choice of the metric parameters.

4. Adaptive data generation using FFT-based microstructure models

4.1. Motivation

In this section, we consider the more realistic scenario in which only an incomplete or even empty data set is available. We perform virtual experiments using a computational microstructure model (in the following also called representative volume element (RVE) model), using its homogenized stress and strain response as data points. Since we use the data from the RVE model directly in the macroscopic boundary value problem, we ensure that the material response is "ground-truth" and not affected by possibly wrong material model predictions. Of course, the "ground-truth" of the microstructure model is also assumption which has to be validated in real-world applications. However, computational RVE models offer a convenient way to systematically improve the accuracy of the complex material behavior by means of refinement of the RVE.

In particular, we develop a systematic and automated scheme for enriching a data set in order to solve a boundary value problem with a data-driven solver scheme with a desired accuracy, while minimizing the number of costly RVE evaluations. One advantage of the direct data-driven paradigm is that a data-driven solution, *i.e.*, an optimal assignment of data points to material points, provides a direct measure of the data that is missing in order to fulfill equilibrium and kinematical compatibility for a given boundary value problem. Using this information leads to a so-called goal-oriented data generation scheme since it generates data for a specific BVP [15]. Nevertheless, this data may also be useful for further, different subsequent loading conditions or different BVPs with the same material.

This paper considers the behavior of a rate-independent plastic material. However, unloading is not considered, as the focus is on the performance of the data generation scheme, which is isolated from the effects of a history parametrization for the data-driven solver scheme. It is important to note that even simple loading is path-dependent, and thus the entire loading path must be considered when evaluating the RVE.

4.2. Proposed method: Adaptive data generation

The general procedure of the proposed method is as follows: Step (1) Given the current data set compute a data-driven solution. Step (2) Compute new proposal strain paths using the given information of data, equilibrium, and compatibility. Step (3) Cluster these strain paths to avoid duplicate RVE evaluations using the error measurement. Step (4) Evaluate RVE with clustered strain paths and add the new stress–strain paths to the data set. Then repeat until desired tolerance is achieved. The following subsections provide the details for each step.

4.2.1. Step (1) Data-driven solution

To compute the optimal assignment of data points to material points we use the randomized solver scheme proposed in Section 3. Since a sequence of loadings is applied to the BVP, we label each solution by a time index $t \in [1, 2, \dots, T]$ as $(\varepsilon'_t, \sigma'_t)$ and $(\varepsilon_t, \sigma_t)$, thus obtaining *path data*. Recall that $(\varepsilon'_t, \sigma'_t) \in D$ is the optimal data field and $(\varepsilon_t, \sigma_t) \in E$ the closest admissible strain and stress field w.r.t. to that assignment of data. We indicate path data by an underline, for instance one local, compatible, strain path is denoted by $\underline{\varepsilon}_e = (\varepsilon_{e,1}, \varepsilon_{e,2}, \dots, \varepsilon_{e,T})$. We also store the local error $F_{e,t} = \|\varepsilon'_{e,t} - \varepsilon_{e,t}\|^2 + \|\sigma'_{e,t} - \sigma_{e,t}\|^2$ at every material point e in every time step t.

4.2.2. Step (2) Strain paths proposals

We propose to store and use the homogenized material tangent information of the RVE, which may be either computed analytically or by means of strain perturbations. For each data point $(\varepsilon'_t, \sigma'_t) \in D_e$ the measured tangent is denoted by T'_t. Then, we denote the tangent associated to the local data point assignment $(\varepsilon'_{e,t}, \sigma'_{e,t}) \in D_e$ of material point e at time t by $T'_{e,t}$. The whole tangent field corresponding to the assignment $(\varepsilon'_t, \sigma'_t) \in D$ is then denoted by T'_t. Using the tangent information allows us to evaluate the RVE in a purely strain-driven manner, even in a force-driven BVP, which is easy to implement and always available in contrast to mixed-loading RVE evaluations.

We now compute proposal strain fields ε^*_t for each time step t independently, in such a way that each is kinematically compatible, and the associated tangent stress field is in equilibrium. Kinematical compatibility is ensured by expressing $\varepsilon^*_t = B_{\text{red}} u_{\text{red},t} + \varepsilon_t$. The associated tangential stress field around the computed data field $(\varepsilon'_t, \sigma'_t)$ is then given by $\sigma(u_{\text{red},t}) = \sigma'_t + T'_t(B_{\text{red}} u_{\text{red},t} + \varepsilon_t - \varepsilon'_t)$. We enforce equilibrium by the discretized equilibrium equation $B^T_{\text{red}} W \sigma(u_{\text{red},t}) = f_{\text{red}}$. After inserting we obtain

$$\left(B^T_{\text{red}} W T'_t B_{\text{red}}\right) u^*_{\text{red},t} = f_{\text{red}} - B^T_{\text{red}} W \left(\sigma'_t + T'_t(\varepsilon_t - \varepsilon'_t)\right) \tag{9}$$

which can be solved for $u^*_{\text{red},t}$ and thus gives the proposal strain paths $\underline{\varepsilon}^* = \{\underline{\varepsilon}^*_e\}^m_{e=1} = (\varepsilon^*_t : t \in [1, T], \varepsilon^*_t = B_{\text{red}} u^*_{\text{red},t} + \varepsilon_t)$.

The underlying assumption for this approach is, that the material behavior in the neighborhood of a data point $(\varepsilon'_i, \sigma'_i)$ is close to its material tangent T'_i. It is important to note that this procedure serves only to compute the proposal strain paths in an hopefully optimal manner for the RVE evaluations, *i.e.* no extrapolated stress–strain data is included in the data set, but only actually measured data.

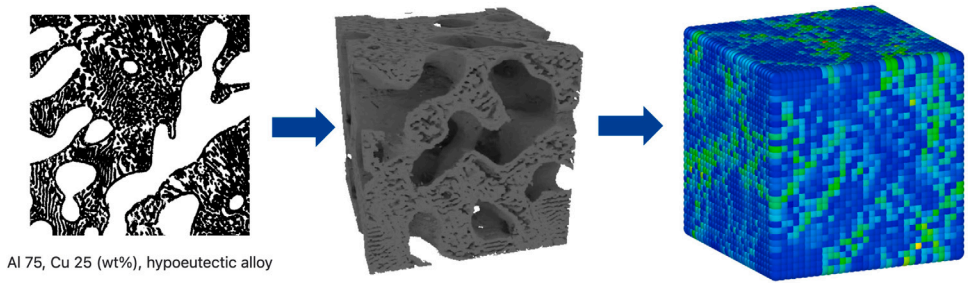

Fig. 3. Workflow for the generation of the FFT model using SliceGAN (https://microlib.io) [46,47]: (1) real image of a microstructure (2) generated 3D microstructure from a trained GAN (3) downsampled FFT-model with 32^3 pixels showing a strain field.

4.2.3. Step (3) Error-weighted clustering

For each local proposal strain path $\underline{\varepsilon}_e^*$ we define a weight which accounts for the error of the material point observed during the data-driven computation by

$$p_e = \exp\left(\frac{1}{\alpha}\sum_{t=1}^{T}(F_{e,t})\right) - 1, \quad \alpha = \frac{1}{m}\sum_{e=1}^{m}\sum_{t=1}^{T}(F_{e,t}). \tag{10}$$

Using this information, we employ a *weighted* k-means cluster algorithm [39] to cluster the strain paths using the weights p_e in order to give more importance to paths with larger error, with the result

$$\bar{\underline{\varepsilon}}_k^* = \frac{\sum_{e\in S_k} p_e \underline{\varepsilon}_e^*}{\sum_{e\in S_k} p_e}, \quad k = 1 \dots K \tag{11}$$

where $\bigcup_{k=1}^{K} S_k$ is the partition of all material points which minimizes the variance

$$\sum_{k=1}^{K}\sum_{e\in S_k} p_e \|\underline{\varepsilon}_e^* - \bar{\underline{\varepsilon}}_k^*\|^2. \tag{12}$$

For the sake of compactness we do not provide the details of the well-known (weighted) k-means clustering as mainstream libraries [40] provide implementations which can be directly used without any modification.

The result of the k-means algorithm are the cluster centers $\{\bar{\underline{\varepsilon}}_k^*\}_{k=1}^K \leftarrow \texttt{KMeans}(\{\underline{\varepsilon}_e^*, p_e\}_{e=1}^m)$. Instead of using these cluster centers for the evaluation of the RVE we use the proposal strain path which are the nearest to each cluster center. This operation is performed by the nearest neighbor search

$$\underline{\varepsilon}_k^* = \arg\min_{\underline{\varepsilon}_e^* \in \underline{\varepsilon}^*} \|\underline{\varepsilon}_e^* - \bar{\underline{\varepsilon}}_k^*\|^2, \quad \text{for } k = 1 \dots K. \tag{13}$$

The number of clusters K has to be set in advance. Given the number of material points m, we prescribe a certain cluster ratio $r = K/m$ from which K follows. We will study the influence of the cluster ratio in the numerical example 4.4.

4.2.4. Step (4) RVE evaluation

Finally, we compute the new stress data associated to the strain paths $\{\underline{\varepsilon}_k^*\}_{k=1}^K$. We perform the RVE evaluations using the Fast-Fourier-Transform (FFT) based fixed point algorithm proposed by [41]. More efficient solver schemes [42] are available for even faster evaluation times. For a review of the state of the art of these solvers and the computation of material tangents we refer to [43–45]. The FFT based solver schemes are efficient for the evaluation of periodic microstructures and can be conveniently evaluated with the strain paths without the need to compute an equivalent displacement loading. In the solver scheme, a reference stiffness $\mathbb{C}_0$ has to be defined, usually as the average elastic stiffness matrix of each constituent. For convenience, we use this reference stiffness also as the metric coefficients $\mathbb{C}_e$ of the data-driven solver scheme.

The availability and acquisition of realistic three-dimensional microstructures is still limited and subject to research. In this work, we obtained a sample from the public online library Microlib [46] which is based on a generative adversarial network (GAN) architecture that generates 3D microstructures based on real images of microstructure slices [47]. The workflow for generating the FFT model used in the following using this method is visualized in Fig. 3

4.3. Algorithm summary

The proposed adaptive data generation algorithm is summarized in Algorithm 3.

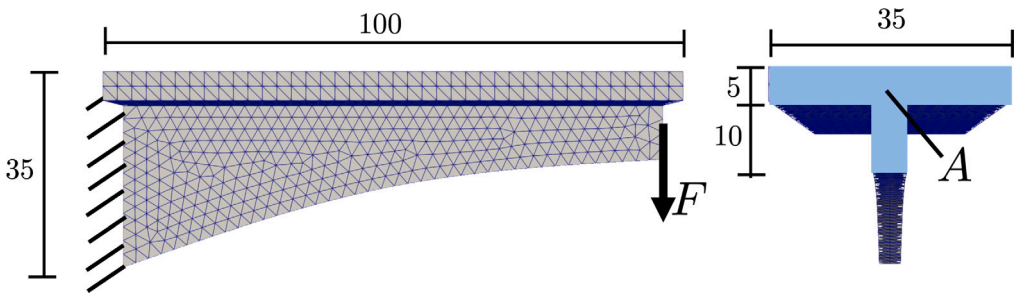

Fig. 4. Beam boundary value problem.

Algorithm 3 Adaptive data generation

Require: Constraint set(s) E_t.
Require: Initial local data set(s) with tangents $D_e = \{(0, 0, T_0')\}$.
Require: Target error tolerance `tol`
  Initialize: $it \leftarrow 0$
  while $F_{99\%} >$ `tol` **do**
    for $t = 1 \dots T$ **do**
      Set: $\varepsilon_t, \sigma_t, \varepsilon_t', \sigma_t', F_t \leftarrow$ `Min_Dist`(E_t, D_e)
      Solve Eq. (9) for $u^*_{\text{red,t}}$
      Set: $\varepsilon^*_t \leftarrow B_{\text{red}} u^*_{\text{red,t}} + \varepsilon_t$
    end for
    Set: $F_{99\%} \leftarrow$ `percentile`$(F_{e,t}, 99)$
    Set: p_e (Eq. (10))
    Set: $K =$ `int`$(r(it) * m)$ # cluster ratio * number of material points
    Set: $\{\bar{\underline{\varepsilon}}^*_k\}_{k=1}^K \leftarrow$ `KMeans`$(\underline{\varepsilon}^*,$ `sample_weights` $= p_e)$
    Set: $\underline{\varepsilon}^*_k \leftarrow \arg\min_{\underline{\varepsilon}^*_e \in \underline{\varepsilon}^*} \|\underline{\varepsilon}^*_e - \bar{\underline{\varepsilon}}^*_k\|^2$
    for $k = 1 \dots K$ **do**
      Set: $\underline{\sigma}^*_k, \underline{T}^*_k \leftarrow$ `RVE`$(\underline{\varepsilon}^*_k)$
      Set: $D_e \leftarrow D_e \cup (\underline{\varepsilon}^*_k, \underline{\sigma}^*_k, \underline{T}^*_k)$
    end for
    Set: $it \leftarrow it + 1$
  end while
  return D_e

4.4. Numerical example: Beam

4.4.1. Setup

As a numerical example, we consider the beam shown in Fig. 4. The monotonically increasing force $F(t)$ is distributed over the surface A as $F(t) = \int_A 5 \frac{t}{[s]} da$ [MN] for time $t \in (0, 1)[s]$ within 20 time steps, having the whole left edge of the beam clamped in all directions. The mesh consists of 13,753 linear tetrahedral elements.

We assume homogeneous material behavior over the structure and no randomization of the microstructure, *i.e.* the material behavior of every material point is described by the same RVE. The RVE is resolved by 32^3 pixels as shown in Fig. 3 and contains two phases, Aluminium and Copper. We assume that the material behavior of each phase is less complex than the overall response of the RVE and can thus be described by a Von-Mises plasticity model with isotropic hardening. The material parameters for the two phases are chosen as follows: $E_{\text{Al}} = 68000$[MPa], $\nu_{\text{Al}} = 0.36, \sigma_{y0,\text{Al}} = 240$[MPa], $H_{\text{Al}} = E_{\text{Al}}/1000$ and $E_{\text{Cu}} = 110000$[MPa], $\nu_{\text{Cu}} = 0.343, \sigma_{y0,\text{Cu}} = 33.3$[MPa], $H_{\text{Cu}} = E_{\text{Cu}}/1000$.

4.4.2. Results

We evaluate the performance of the proposed adaptive data generation scheme for different cluster ratios. Every simulation starts with a data set containing only a zero data point and is iterated until the error tolerance 10^{-5} is achieved. For this, we measure the 99-percentile error $F_{99\%}$ of all local errors $F_{e,t}$. This error measure is much stricter than for instance the mean or median of all local errors, but excludes a small fraction of maximum errors which tend to fluctuate due to inaccuracies of the data-driven solver scheme.

First, we have run the adaptive data generation scheme for the cluster ratios $r = 1\%$ and $r = 10\%$. The error over the data set size is shown in Fig. 5. For a better comparison, we also provide the data set size per number of material points and time steps. We

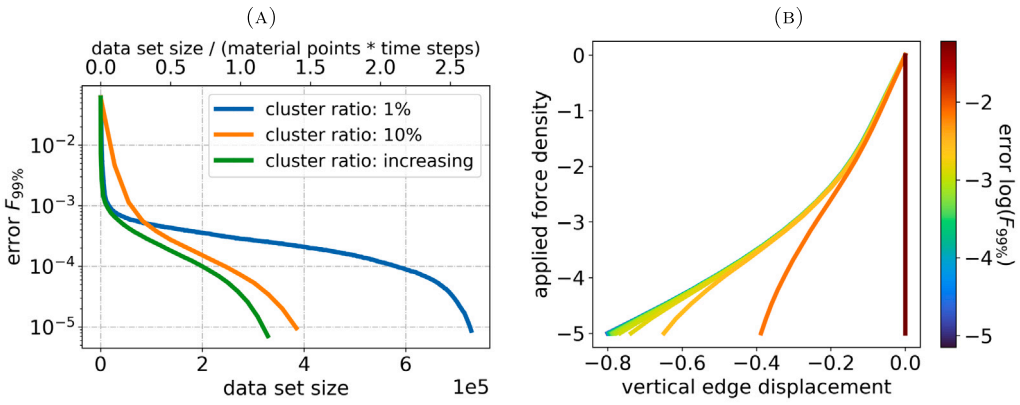

Fig. 5. (A) 99-percentile error for the iteratively enriched data sets using different cluster ratios. (B) Force–Displacement curve for different iterations of data generation. Colored by the logarithm of the 99-percentile error.

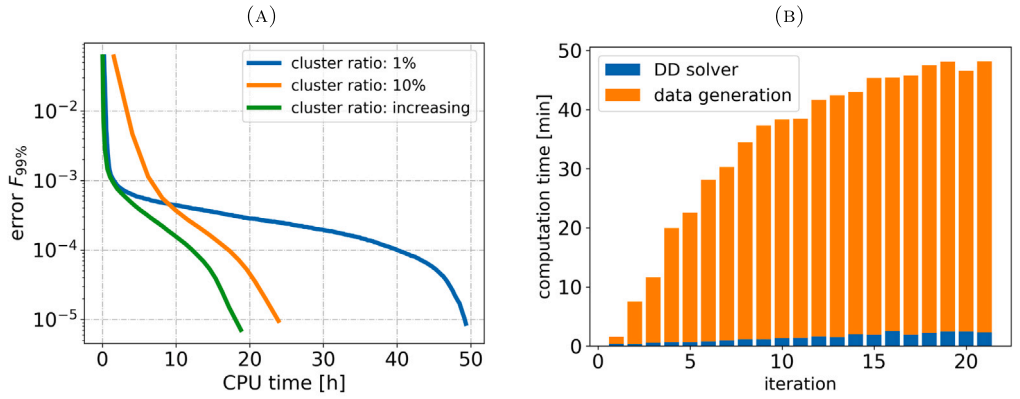

Fig. 6. (A) CPU times for the different cluster ratios. (B) CPU times per iteration for the increasing cluster ratio scheme until a accuracy of $F_{99\%} < 10^{-4}$ is reached.

observe that it is much more efficient to add very few data (*i.e.* a cluster ratio of 1%) in the first iterations instead of adding larger amounts of data. The reason for this is that at this stage the strain paths are not yet converged and thus the generated data cannot be reused in later iterations. However, once the system has reached a certain level of convergence (the cutting point of the orange and blue line in Fig. 5 A)) a higher cluster ratio is more efficient, since a strong clustering smears out the accurately requested proposal paths too much. This motivates our suggestion to start slowly by adding very little data, but then successively increasing the cluster ratio. Based on this we have run the scheme using a successively increasing cluster ratio defined by the heuristic formula

$$r(it) = [0.1 + (1 - e^{(-it/20)})(10 - 0.1)]\% \tag{14}$$

where it is the iteration number and 0.1% and 10% chosen starting and final cluster ratios, respectively. As shown in Fig. 5 (A) by the green curve this increasing cluster ratio scheme achieves the best results, *i.e.* achieves any error level with a minimum amount of data.

In order to assess what is a reasonable error level we evaluate the macroscopic response of the system as shown in Fig. 5 (B). Here, we measure the average, vertical displacement of the right edge of the beam as function of the applied force density. From this, we conclude visually that an error range in the order of $F_{99\%} \sim 10^{-3}$–10^{-4} results in a converged macroscopic system response.

The measured CPU times (as computed on a 24 cores shared cluster node) are reported in Fig. 6. We note that, for sufficiently large and realistic RVEs, the CPU time correlates directly to the amount of generated data, rather than to the number of iterations of data generation. The reason for this is, that the data-driven solving time compared to the data generation time is much smaller, as shown in Fig. 6 (B) for the increasing cluster ratio scheme. Note that the clustering is performed in the order of a few seconds, and it is computing time thus neglectable. Choosing a reasonable target tolerance of $F_{99\%} = 10^{-4}$ the overall computational cost is approximate 12 h, thus enabling the solving of the three-dimensional multiscale problem in an acceptable time.

Finally, we compare the performance of the newly proposed randomized fixed-point solver scheme to the original solver as shown in Fig. 7. In addition to the 99-percentile error, we show the maximum error $F_{\max} = \max F_{e,t}$, *i.e.* the maximum local error of all material points and times steps. The randomized solver clearly outperforms the original solver by efficiently escaping local minima.

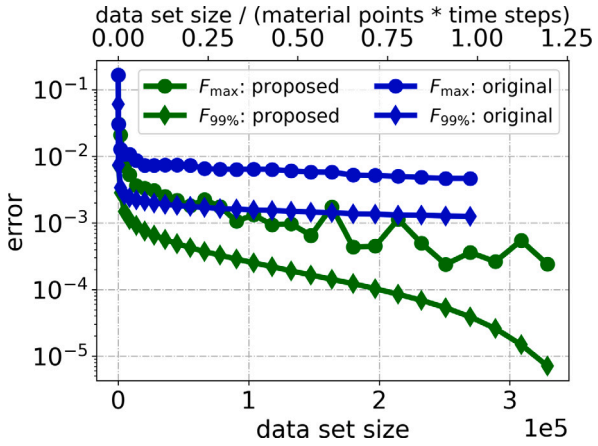

Fig. 7. Comparison of the original and the newly proposed randomized fixed-point solver schemes for the increasing cluster ratio. In addition to the 99-percentile error, the maximum error is shown.

5. Summary and concluding remarks

We have presented two algorithms, an accurate solver algorithm and a strategy for adaptive data generation. Both have been shown to lead to significant improvements for relevant, three-dimensional multiscale problems.

The proposed solver algorithm is easy to implement and requires only minimal changes from the original solver algorithm. However, it can significantly improve the accuracy. This is achieved by searching separately for stresses and strains, thus effectively removing the impact of choice for metric coefficients. By randomization, local minima can be efficiently escaped. Since no additional nearest neighbor searches or other operations are performed, we observe no additional computational costs.

Based on this solver, we developed a new adaptive data generation algorithm using the material tangent information and an error-weighted k-means clustering. This automated and systematic approach to dataset enrichment has consistently minimized errors. For the numerical example under study, we have reached an acceptable error level at a dataset size below the number of material points times the number of time steps. In comparison to a classical inelastic finite element computation, where the RVE must be evaluated multiple times per time step, the proposed method demonstrates significant potential. We anticipate the benefits to be even more substantial when multiple boundary value problems are computed, allowing for the reuse of previously computed data.

The error-weighted k-means clustering guidance for RVE evaluations can also be beneficial for model-based schemes. In this context, it can be used to validate the material model for predictions in regions without measured data by optimal selected, limited RVE evaluations. Using this for future works, a fair comparison between a model-based and direct data-driven scheme can be performed. While the clustering algorithm already incorporates strain path RVE evaluations, future works need to include history dependent data-driven solvers [18] in order to compute unloading scenarios. Finally, the proposed method can be extended to data from randomized microstructures and potentially from different pixel resolution levels for uncertainty quantification purposes.

CRediT authorship contribution statement

E. Prume: Writing – original draft, Visualization, Software, Methodology, Investigation, Data curation. **C. Gierden:** Writing – review & editing, Methodology. **M. Ortiz:** Writing – review & editing, Supervision, Methodology, Funding acquisition, Conceptualization. **S. Reese:** Supervision, Project administration, Funding acquisition, Conceptualization.

Declaration of competing interest

The authors declare that they have no known competing financial interests or personal relationships that could have appeared to influence the work reported in this paper.

Acknowledgments

EP thanks Kevin Linka for very helpful discussions. EP, CG and SR gratefully acknowledge the financial support of the Deutsche Forschungsgemeinschaft (DFG), Germany through the project "Multiscale modeling based on a novel combination of direct data-driven methods with Fourier transform-based microstructure simulation" (RE 1057/58-1, project number 532163998). MO gratefully acknowledges the support of the Deutsche Forschungsgemeinschaft (DFG, German Research Foundation) *via* project 211504053 - SFB 1060; project 441211072 - SPP 2256; and project 390685813 - GZ 2047/1 - HCM.

Data availability

Data will be made available on request.

References

[1] Marc G.D. Geers, Varvara G. Kouznetsova, W. Brekelmans, Multi-scale computational homogenization: Trends and challenges, J. Comput. Appl. Math. 234 (7) (2010) 2175–2182.

[2] Jacob Fish, Gregory J. Wagner, Sinan Keten, Mesoscopic and multiscale modelling in materials, Nat. Mater. 20 (6) (2021) 774–786.

[3] Frédéric Feyel, Jean-Louis Chaboche, FE2 multiscale approach for modelling the elastoviscoplastic behaviour of long fibre SiC/Ti composite materials, Comput. Methods Appl. Mech. Engrg. 183 (3–4) (2000) 309–330.

[4] Mohamed Amine Benaimeche, Julien Yvonnet, Benoit Bary, Qi-Chang He, A k-means clustering machine learning-based multiscale method for anelastic heterogeneous structures with internal variables, Internat. J. Numer. Methods Engrg. 123 (9) (2022) 2012–2041.

[5] Kevin Linka, Markus Hillgärtner, Kian P. Abdolazizi, Roland C. Aydin, Mikhail Itskov, Christian J. Cyron, Constitutive artificial neural networks: A fast and general approach to predictive data-driven constitutive modeling by deep learning, J. Comput. Phys. 429 (2021) 110010.

[6] Faisal As' ad, Philip Avery, Charbel Farhat, A mechanics-informed artificial neural network approach in data-driven constitutive modeling, Internat. J. Numer. Methods Engrg. 123 (12) (2022) 2738–2759.

[7] Filippo Masi, Ioannis Stefanou, Paolo Vannucci, Victor Maffi-Berthier, Thermodynamics-based artificial neural networks for constitutive modeling, J. Mech. Phys. Solids 147 (2021) 104277.

[8] Hagen Holthusen, Lukas Lamm, Tim Brepols, Stefanie Reese, Ellen Kuhl, Theory and implementation of inelastic constitutive artificial neural networks, Comput. Methods Appl. Mech. Engrg. 428 (2024) 117063.

[9] Xin Liu, Su Tian, Fei Tao, Wenbin Yu, A review of artificial neural networks in the constitutive modeling of composite materials, Composites B 224 (2021) 109152.

[10] Jan Niklas Fuhg, Govinda Anantha Padmanabha, Nikolaos Bouklas, Bahador Bahmani, WaiChing Sun, Nikolaos N. Vlassis, Moritz Flaschel, Pietro Carrara, Laura De Lorenzis, A review on data-driven constitutive laws for solids, 2024, arXiv preprint arXiv:2405.03658.

[11] Jan Niklas Fuhg, Christoph Böhm, Nikolaos Bouklas, Amelie Fau, Peter Wriggers, Michele Marino, Model-data-driven constitutive responses: Application to a multiscale computational framework, Internat. J. Engrg. Sci. 167 (2021) 103522.

[12] Karl A. Kalina, Lennart Linden, Jörg Brummund, Markus Kästner, FE ANN: an efficient data-driven multiscale approach based on physics-constrained neural networks and automated data mining, Comput. Mech. 71 (5) (2023) 827–851.

[13] T. Kirchdoerfer, M. Ortiz, Data-driven computational mechanics, Comput. Methods Appl. Mech. Engrg. 304 (2016) 81–101.

[14] Tim Fabian Korzeniowski, Kerstin Weinberg, A multi-level method for data-driven finite element computations, Comput. Methods Appl. Mech. Engrg. 379 (2021) 113740.

[15] Anna Gorgogianni, Konstantinos Karapiperis, Laurent Stainier, Michael Ortiz, José E. Andrade, Adaptive goal-oriented data sampling in data-driven computational mechanics, Comput. Methods Appl. Mech. Engrg. 409 (2023) 115949.

[16] Lu Trong Khiem Nguyen, Marc-André Keip, A data-driven approach to nonlinear elasticity, Comput. Struct. 194 (2018) 97–115.

[17] Auriane Platzer, Adrien Leygue, Laurent Stainier, Michael Ortiz, Finite element solver for data-driven finite strain elasticity, Comput. Methods Appl. Mech. Engrg. 379 (2021) 113756.

[18] R. Eggersmann, T. Kirchdoerfer, S. Reese, L. Stainier, M. Ortiz, Model-free data-driven inelasticity, Comput. Methods Appl. Mech. Engrg. 350 (2019) 81–99.

[19] Pietro Carrara, Laura De Lorenzis, Laurent Stainier, Michael Ortiz, Data-driven fracture mechanics, Comput. Methods Appl. Mech. Engrg. 372 (2020) 113390.

[20] Xu Guo, Zongliang Du, Chang Liu, Shan Tang, A new uncertainty analysis-based framework for data-driven computational mechanics, J. Appl. Mech. 88 (11) (2021) 111003.

[21] Selina Zschocke, Ferenc Leichsenring, Wolfgang Graf, Michael Kaliske, A concept for data-driven computational mechanics in the presence of polymorphic uncertain properties, Eng. Struct. 267 (2022) 114672.

[22] Erik Prume, Stefanie Reese, Michael Ortiz, Model-free data-driven inference in computational mechanics, Comput. Methods Appl. Mech. Engrg. 403 (2023) 115704.

[23] Robert Eggersmann, Laurent Stainier, Michael Ortiz, Stefanie Reese, Model-free data-driven computational mechanics enhanced by tensor voting, Comput. Methods Appl. Mech. Engrg. 373 (2021) 113499.

[24] Kerem Ciftci, Klaus Hackl, Model-free data-driven simulation of inelastic materials using structured data sets, tangent space information and transition rules, Comput. Mech. 70 (2) (2022) 425–435.

[25] Herbert De Gersem, Armin Galetzka, Ion Gabriel Ion, Dimitrios Loukrezis, Ulrich Römer, Magnetic field simulation with data-driven material modeling, IEEE Trans. Magn. 56 (8) (2020) 1–6.

[26] Eduard Marenić, Guillem Seychal, Jean-Charles Passieux, Data driven approach in multiphysics framework: Application to coupled electro-mechanical problems, Comput. Methods Appl. Mech. Engrg. 395 (2022) 114959.

[27] Adrien Leygue, Michel Coret, Julien Réthoré, Laurent Stainier, Erwan Verron, Data-based derivation of material response, Comput. Methods Appl. Mech. Engrg. 331 (2018) 184–196.

[28] Moritz Flaschel, Siddhant Kumar, Laura De Lorenzis, Discovering plasticity models without stress data, npj Comput. Mater. 8 (1) (2022) 91, arXiv:2202.04916 [cs].

[29] Marie Dalémat, Michel Coret, Adrien Leygue, Erwan Verron, Measuring stress field without constitutive equation, Mech. Mater. 136 (2019) 103087.

[30] Tung-Huan Su, Nian-Hu Lu, Chih-Hsuan Chen, Chuin-Shan Chen, Full-field stress and strain measurements revealing energy dissipation characteristics in martensitic band of Cu-Al-Mn shape memory alloy, Mater. Today Commun. 24 (2020) 101321.

[31] Raphaël Langlois, Michel Coret, Julien Réthoré, Non-parametric stress field estimation for history-dependent materials: Application to ductile material exhibiting Piobert–Lüders localization bands, Strain 58 (4) (2022) e12410.

[32] Ante Buljac, Clément Jailin, Arturo Mendoza, Jan Neggers, Thibault Taillandier-Thomas, Amine Bouterf, Benjamin Smaniotto, François Hild, Stéphane Roux, Digital volume correlation: review of progress and challenges, Exp. Mech. 58 (2018) 661–708.

[33] Hossein Salahshoor, Michael Ortiz, Model-free data-driven viscoelasticity in the frequency domain, Comput. Methods Appl. Mech. Engrg. 403 (2023) 115657.

[34] Yoshihiro Kanno, Mixed-integer programming formulation of a data-driven solver in computational elasticity, Optim. Lett. 13 (7) (2019) 1505–1514, arXiv:1810.04394.

[35] Armin Galetzka, Dimitrios Loukrezis, Herbert De Gersem, Data-driven solvers for strongly nonlinear material response, Internat. J. Numer. Methods Engrg. 122 (6) (2021) 1538–1562, arXiv:2008.08482.

[36] Lu Trong Khiem Nguyen, Roland Can Aydin, Christian Johannes Cyron, Accelerating the distance-minimizing method for data-driven elasticity with adaptive hyperparameters, Comput. Mech. 70 (3) (2022) 621–638.
[37] Tim Fabian Korzeniowski, Kerstin Weinberg, A multi-level method for data-driven finite element computations, Comput. Methods Appl. Mech. Engrg. (2021).
[38] Armin Galetzka, Dimitrios Loukrezis, Herbert De Gersem, Data-driven solvers for strongly nonlinear material response, Internat. J. Numer. Methods Engrg. 122 (6) (2021) 1538–1562.
[39] Stuart Lloyd, Least squares quantization in PCM, IEEE Trans. Inform. Theory 28 (2) (1982) 129–137.
[40] F. Pedregosa, G. Varoquaux, A. Gramfort, V. Michel, B. Thirion, O. Grisel, M. Blondel, P. Prettenhofer, R. Weiss, V. Dubourg, J. Vanderplas, A. Passos, D. Cournapeau, M. Brucher, M. Perrot, E. Duchesnay, Scikit-learn: Machine learning in Python, J. Mach. Learn. Res. 12 (2011) 2825–2830.
[41] Hervé Moulinec, Pierre Suquet, A numerical method for computing the overall response of nonlinear composites with complex microstructure, Comput. Methods Appl. Mech. Engrg. 157 (1–2) (1998) 69–94.
[42] Matthias Kabel, Thomas Böhlke, Matti Schneider, Efficient fixed point and Newton–Krylov solvers for FFT-based homogenization of elasticity at large deformations, Comput. Mech. 54 (6) (2014) 1497–1514.
[43] Matti Schneider, A review of nonlinear FFT-based computational homogenization methods, Acta Mech. 232 (6) (2021) 2051–2100.
[44] Christian Gierden, Julian Kochmann, Johanna Waimann, Bob Svendsen, Stefanie Reese, A review of FE-FFT-based two-scale methods for computational modeling of microstructure evolution and macroscopic material behavior, Arch. Comput. Methods Eng. 29 (6) (2022) 4115–4135.
[45] Felix Selim Göküzüm, Marc-André Keip, An algorithmically consistent macroscopic tangent operator for FFT-based computational homogenization, Internat. J. Numer. Methods Engrg. 113 (4) (2018) 581–600.
[46] Steve Kench, Isaac Squires, Amir Dahari, Samuel J. Cooper, MicroLib: A library of 3D microstructures generated from 2D micrographs using slicegan, Sci. Data 9 (1) (2022) 645.
[47] Steve Kench, Samuel J. Cooper, Generating three-dimensional structures from a two-dimensional slice with generative adversarial network-based dimensionality expansion, Nat. Mach. Intell. 3 (4) (2021) 299–305.